RSC Advances

PAPER

View Article Online
View Journal | View Issue

Cite this: RSC Adv., 2014, 4, 48876

Influence of push–pull configuration on the electro-optical and charge transport properties of novel naphtho-difuran derivatives: a DFT study†

Aijaz Rasool Chaudhry,*[ab] R. Ahmed,*[a] Ahmad Irfan,[c] Shabbir Muhammad,[b] A. Shaari[a] and Abdullah G. Al-Sehemi[cde]

We present a density functional theory (DFT) study pertaining to electro-optical and charge transport properties of two novel derivatives of diphenyl-naphtho[2,1-*b*:6,5-*b*′]difuran (DPNDF) as investigated based on push-pull configuration. Both molecular structures of the designed derivatives were optimized, in ground state (S_0) as well as excited state (S_1), using DFT and time-dependent DFT (TD-DFT) respectively. The push-pull configuration effect was studied meticulously for different electro-optical properties including adiabatic/vertical electron affinity (EAa/EAv), adiabatic/vertical ionization potential (IPa/IPv) and hole/electron reorganization energies (λ_h/λ_e), hole/electron transfer integrals (V_h/V_e), hole/electron mobility and photostability. We observed smaller λ_e, improved V_e and higher electron mobility for compound **1** compared with the parent molecule. Our calculated value of the electron mobility for compound **1** (2.43 $cm^2\ V^{-1}\ s^{-1}$) revealed it to be an efficient electron transport material. Moreover, the influence of the push-pull on the electronic structure was also investigated by calculating the total and partial density of states (DOS). Taking advantage of the strong push-pull configurations effect on other properties, the study of the designed chemical systems was extended to their nonlinear optical (NLO) properties. Our designed novel derivatives (**1** & **2**) exhibited significantly larger amplitude values for first hyperpolarizability with β_{tot} equal to 209.420 $\times\ 10^{-30}$ esu for compound **1** and 333.830 $\times\ 10^{-30}$ esu for compound **2**. It was found that the first hyperpolarizability and HOMO–LUMO energy gap are in an inverse relationship for compounds **1** and **2**.

Received 17th June 2014
Accepted 19th September 2014

DOI: 10.1039/c4ra05850j

www.rsc.org/advances

1. Introduction

Push–pull is an important strategy widely used in organic semiconductor materials (OSMs) to tune the photophysical properties.[1–4] More recently, the push–pull strategy has been a good approach for enhancing the electronic and charge transport properties.[5–8] A stronger push–pull effect represents a significant charge separation on molecular geometry and dipole moment.[6] A push–pull configuration usually consists of an electron donating group (EDG), a π conjugation bridge and an electron withdrawing group (EWG), which is expressed as EDGs-π-EWGs. Such a type of push–pull configuration with strong EDGs and EWG results in lowering the HOMO–LUMO energy gap E_g, which leads to efficient intramolecular charge transfer[9] and material performance that is beneficial for designing excellent OSMs. OSMs with push–pull configuration[10–12] are widely studied at both levels (theoretical and experimental) due to their light weight and their low fabrication cost on flexible substrates and large area bendy displays. These advantages of OSMs give them an edge over the silicon-based traditional inorganic semiconductors and have attracted massive interest of academic researchers as well as their industrial partners because of their potential applications in photonics and electronic devices, such as organic field effect transistors (OFETs),[13–15] organic light emitting diodes (OLEDs),[16,17] organic photo-voltaics (OPVs)[17,18] and organic light emitting transistors (OLETs).[19]

OFETs are fabricated and produced by adding an electron system with π-conjugation,[20] or an aromatic compound[21] which helps in the orbital wave functions delocalization[22] and establishes a good relationship between the geometric and electronic structure.[23–28] Several experimental and theoretical research reports are available on thiophene containing materials for use

[a]Department of Physics, Faculty of Science, Universiti Teknologi Malaysia, UTM Skudai, 81310 Johor, Malaysia. E-mail: aijaz_bwp27@hotmail.com; rashidahmed@utm.my; Tel: +60 17 734 1953

[b]Department of Physics, Faculty of Science, King Khalid University, P.O. Box 9004, Abha 61413, Saudi Arabia

[c]Department of Chemistry, Faculty of Science, King Khalid University, P.O. Box 9004, Abha 61413, Saudi Arabia

[d]Unit of Science and Technology, Faculty of Science, King Khalid University, P.O. Box 9004, Abha 61413, Saudi Arabia

[e]Center of Excellence for Advanced Materials Research, King Khalid University, P.O. Box 9004, Abha 61413, Saudi Arabia

† Electronic supplementary information (ESI) available. See DOI: 10.1039/c4ra05850j

in OFETs and OLEDs.[29–38] The push–pull effect on the electronic, optical and charge transport properties of the benzo[2,3-*b*]thiophene derivatives has been studied theoretically.[6] However, in the literature only a very small number of investigations has been reported about the furan containing OFETs and OLEDs materials.[39–42] Considerable attention is currently being given to furan as a basic building block for organic π-conjugated materials that are more stable and that have given an indication of their potential applications, especially in OFETs and OLEDs.[19,43–48] Binaphtha-furanyl has been reported as an OLET.[19] Recently, diphenyl-naphtho[2,1-*b*:6,5-*b*′]difuran (DPNDF) has been experimentally synthesized and reported as a good hole transport OSM for OFETs.[49] In our previous study,[50] it was also found that the furan ring is one of the best electron transport materials because it demonstrates very low reorganization energy for electron λ_e.

No study on DPNDF with push–pull strategy has been found in the literature so far. In our present work, as a starting point, the experimental crystal of DPNDF[49] has been used as the parent molecule and two new structures were derived by employing a push–pull approach where EDGs were attached on one side of the naphtho-difuran (NDF) ring and EWGs on the other side (EDGs-π-EWGs). In these structures, three CH_3/OCH_3 groups were attached as EDGs at position X, whereas three CN groups were attached as EWGs at position Y for structures **1**/**2**, respectively (named compound **1** and compound **2**) (see Scheme 1 and Fig. S1 of the ESI†).

The derived geometries were optimized in ground state (S_0) and first excited states (S_1) at the level of DFT and TD-DFT, respectively. Also, the other properties such as highest occupied molecular orbitals (HOMOs), lowest unoccupied molecular orbitals (LUMOs), HOMO–LUMO energy gap (E_g), adiabatic and vertical electron affinities (EAa/EAv), reorganization energies for hole (λ_h)/electron (λ_e), adiabatic/vertical ionization potentials (IPa/IPv), total/partial density of states (TDOS/PDOS), nonlinear optical properties (NLO), hole extraction potential (HEP), electron extraction potential (EEP) and electronegativity (χ) were computed and are discussed in detail. In addition, the transfer integrals, mobility and photostability of these compounds were evaluated. Moreover, the push–pull effect was investigated on the above mentioned properties. A comparison of our obtained results with experimental data is also made where available.

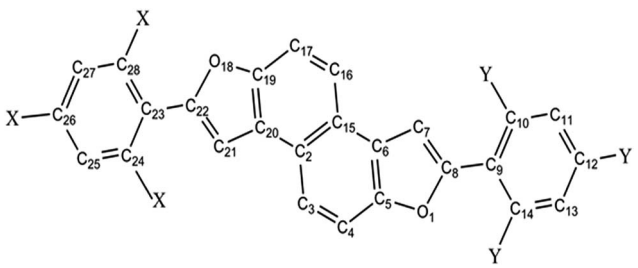

Compound 1; X=CH_3; Y=CN

Compound 2; X=OCH_3; Y=CN

Scheme 1 Labeled diagram of DPNDF showing the positions of the attached groups.

2. Computational methodology

DFT was used to optimize the initial molecular structures for S_0 by applying the hybrid exchange correlation functional B3LYP[51–53] with 6-31G** basis sets.[30,39–42,54–56] For S_1 TD-DFT,[56–59] the hybrid functional TD-B3LYP[60–63] with the same basis set was used to optimize the geometries of the analogues. The electronic and photophysical properties including absorption (λ_{abs}), and emission (λ_{emis}) wavelengths were calculated at the same level of theory. Reorganization energy (λ) represents the geometric relaxation energy of a molecule from the charged (cation/anion) to the neutral state and from neutral to the charged (cation/anion) state (for details see the computational method expressed in the ESI†). The reorganization energy for hole (λ_h) and electron (λ_e) was evaluated as:

$$\lambda_h = \lambda_+ + \lambda_1 \text{ and } \lambda_e = \lambda_- + \lambda_2 \quad (1)$$

where the energy of geometry relaxation from neutral to charged (cation/anion) state is λ_+ and λ_-, and the relaxation energy of a molecule from charged (cation/anion) state to neutral is λ_1 and λ_2, respectively.[64,65] These two terms were calculated directly from the adiabatic potential energy surfaces for λ_h and λ_e.[1,66,67] In the next step, the calculations related to term transfer integrals were performed. To calculate the transfer integrals, intermolecular nearest-neighboring hopping pathways were generated using the single-crystal structure. There are two widely employed approaches to obtain transfer integrals; one is a Koopmans' theorem based method[68] and the other one is a direct evaluation method for the frontier molecular orbitals (FMOs).[69,70] We used the direct approach[69,70] to investigate the charge transport properties in this study. The hole/electron transfer integrals in this approach can be expressed as:

$$t_{h/e} = \langle \phi^{0,site1}_{LUMO/HOMO} | F^0 | \phi^{0,site2}_{LUMO/HOMO} \rangle \quad (2)$$

where $t_{h/e}$ is the hole/electron transfer integrals, $\phi^{0,site1}_{LUMO/HOMO}$ and $\phi^{0,site2}_{LUMO/HOMO}$ correspond to the HOMOs and LUMOs of the two consecutive molecules when there is no contact between the adjacent molecules, and F^0 is the Fock operator with unperturbed molecular orbitals for the dimer of a fixed pathway.

The carrier mobility μ can be evaluated with the help of the Einstein relation as:

$$\mu = eD/k_BT \quad (3)$$

where D represents a charge diffusion constant, e is the electronic charge, T is the temperature and k_B denotes the Boltzmann constant. Further details related to transfer integrals and mobility can be seen in the computational method expressed in the ESI.† All these first-principles calculations were carried out using the GAUSSIAN 09 package.[71]

For investigation of NLO response, we calculated the static first hyperpolarizability (β_{tot}) and its components by a finite field (FF) method. The FF method is broadly applied to investigate NLO because this methodology can be used with the electronic structure method to compute β values.[72–81] In some very recent reports, β_{tot} calculated by this method was found to be substantiated with the experimental structure–property relationship.[10,82] In the FF method, a molecule is subjected to a static electric field (F) and the energy (E) of the molecule is expressed as:

$$E = E^{(0)} - \mu_1 F_1 - \frac{1}{2}\alpha_{ij}F_iF_j - \frac{1}{6}\beta_{ijk}F_iF_jF_k - \frac{1}{24}\gamma_{ijkl}F_iF_jF_kF_l - \ldots \quad (4)$$

where $E^{(0)}$ is the energy of the molecule in the absence of an electronic field, μ is the component of the dipole moment vector, α is the linear polarizability tensor, β and γ are the first and second hyperpolarizability tensors respectively, and i,j and k label the x, y and z components respectively. It is clear from eqn (4) that the values of μ, α, β, and γ can be obtained by differentiating E with respect to F. In our present investigation, we calculated the molecular first hyperpolarizability. For a molecule, the components of the first hyperpolarizability can be calculated using the following:

$$\beta_i = \beta_{iii} + \sum_{i\neq j}\left[\frac{\left(\beta_{ijj} + 2\beta_{jii}\right)}{3}\right] \quad (5)$$

Using the x, y and z components, the magnitude of first hyperpolarizability (β_{tot}) can be calculated by the following:

$$\beta_{tot} = \sqrt{\left(\beta_x^2 + \beta_y^2 + \beta_z^2\right)} \quad (6)$$

where

$$\beta_x = (\beta_{xxx} + \beta_{xxy} + \beta_{xyy}),$$

$$\beta_y = (\beta_{yyy} + \beta_{xxz} + \beta_{yyz}),$$

$$\beta_z = (\beta_{xzz} + \beta_{yzz} + \beta_{zzz})$$

Therefore, the complete equation for calculating the magnitude of the total first static hyperpolarizability from GAUSSIAN 09 outputs is given by:

$$\beta_{tot} = [(\beta_{xxx} + \beta_{xxy} + \beta_{xyy})^2 + (\beta_{yyy} + \beta_{xxz} + \beta_{yyz})^2 + (\beta_{xzz} + \beta_{yzz} + \beta_{zzz})^2]^{1/2} \quad (7)$$

Since these β_{tot} values of the GAUSSIAN 09 output files are reported in atomic units (a.u.), the calculated β_{tot} values were converted into electrostatic units (esu) (1 a.u. = 8.6393×10^{-33} esu). First hyperpolarizability is a third rank tensor that can be described by a $3 \times 3 \times 3$ matrix. The 27 components of the 3D matrix can be reduced to 10 components due to the Kleinman symmetry ($\beta_{xyy} = \beta_{yxy} = \beta_{yyx}$, $\beta_{yyz} = \beta_{yzy} = \beta_{zyy}$,... likewise other permutations also take same value).

3. Results and discussion

3.1. Ground and excited state geometries

The optimized values of bond lengths and bond/dihedral angles for the neutral, cation and anion structures are tabulated in Table S1 of the ESI.† For compound **1**/**2**, the cation and anion structures differ from the neutral one. For compound **1**, alterations in the bond lengths C_{19}–C_{20}, C_{20}–C_{21}, C_{21}–C_{22}, C_{22}–C_{23}, C_{23}–C_{24} and C_{23}–C_{28} were found; for the cation as 0.021 Å, −0.032 Å, 0.37 Å, −0.033 Å, 0.026 Å and 0.023 Å; for the anion as −0.003 Å, 0.00 Å, 0.001 Å, −0.001 Å, 0.004 Å and 0.002 Å, respectively; the bond angles C_{10}–C_9–C_{14}, O_{18}–C_{22}–C_{21} and O_{18}–C_{22}–C_{23} were altered as 1.02°, −1.08° and 1.14° for the cation and as −1.86°, −0.24° and −0.04° for the anion, respectively. Similarly the distortion in the dihedral angles C_{20}–C_{21}–C_{22}–C_{23}, O_{18}–C_{22}–C_{23}–C_{24}, O_{18}–C_{22}–C_{23}–C_{28}, C_{21}–C_{22}–C_{23}–C_{24} and C_{21}–C_{22}–C_{23}–C_{28} was found as −1.13°, 23.23°, −23.53°, −22.09° and 22.40° for the cation and as −0.69°, 4.25°, −4.34°, −3.64° and 3.74° for the anion, respectively, as compared with the neutral ones. A graphical representation of bond lengths in angstrom (Å) for compound **1** (left) and compound **2** (right) is shown in Fig. 1(a) for a more clear understanding of the bond length alteration. The optimized coordinates of the neutral, cation and anion structures for both the compounds are tabulated in Tables S3–S5, respectively, in the ESI.†

For compound **2**, the bond lengths C_9–C_{10}, C_9–C_{14} and C_{11}–C_{12}, varied; for the cation as −0.007 Å, −0.007 Å and 0.00 Å; for the anion as −0.034 Å, 0.031 Å and 0.013 Å, respectively; the bond angles O_1–C_8–C_7, C_8–C_9–C_{14}, C_{10}–C_9–C_{14}, C_{10}–C_{11}–C_{12}, C_{11}–C_{12}–C_{13} and C_{12}–C_{13}–C_{14} were altered as 0.67°, −0.34°, 1.02°, −0.37°, 0.58° and −0.47° for the cation and as −1.19°, 1.08°, −1.83°, 1.32°, −1.50° and 1.09° for the anion, respectively; similarly the distortions in the dihedral angles C_5–C_1–C_8–C_9, C_6–C_7–C_8–C_9, C_1–C_8–C_9–C_{10}, C_1–C_8–C_9–C_{14}, C_7–C_8–C_9–C_{10} and C_7–C_8–C_9–C_{14} were found as 0.37°, 0.66°, −10.12°, 10.12°, 9.39° and −9.40° for the cation and as 1.33°, 1.65°, 17.01°, −16.75°, −18.69° and 18.43° for the anion, respectively, as compared with the neutral ones.

The bond/dihedral angles (degree) are represented graphically for compound **1** (left) and compound **2** (right) in Fig. 1(b), for a more clear understanding of the bond/dihedral angle distortion. The relaxation in the geometric parameters of the compound **1** cation structure was found to be more than that of the anion, whereas for compound **2** the anion had more distortion as compared with the cation. This high distortion especially in bond/dihedral angles[83] might increase the reorganization energy of the compounds due to the increased polarization caused by this distortion. Generally, it has been stated that more relaxation in geometric parameters from neutral to anion/cation can increase the reorganization energy.[2,83]

3.2. Electronic properties

3.2.1 Frontier molecular orbitals (ground and excited states). HOMO and LUMO formation patterns for both the compounds at S_0 and S_1 were formed at isosurface values of 0.02

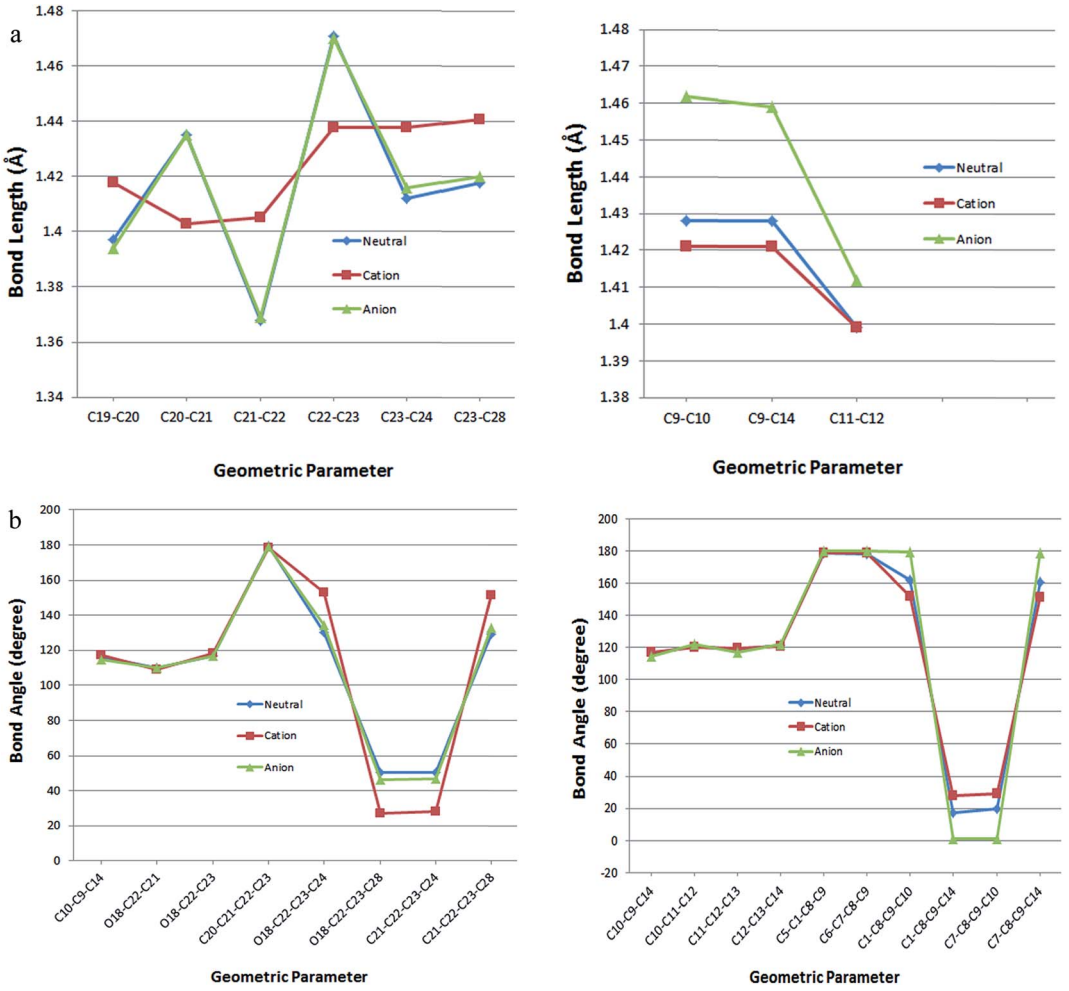

Fig. 1 (a) Selected optimized bond lengths in angstrom (Å) for compound **1** (left) and compound **2** (right) of ground state (neutral, cation and anion) optimized at B3LYP/6-31G** level of theory. (b) Selected optimized bond angles (degree) for compound **1** (left) and compound **2** (right) of ground state (neutral, cation and anion) optimized at B3LYP/6-31G** level of theory.

and are presented in Fig. 2(a) and (b). In compound **1**, for HOMO formation, it was found that the charge is delocalized on C_7–C_8, C_5–C_6, C_3–C_4, C_2–C_{20}–C_{19}, C_{16}–C_{17}, C_{21}–C_{22}, C_{23}–C_{24} and C_{25}–C_{26} while on C_{10}, C_{12} and C_{14} the charge is localized (lone-pair). Neither of the O atoms take part in the formation of the HOMO, whereas a lone-pair is formed on all N atoms. For LUMO formation, the delocalization of charge was found on C_2–C_3, C_5–C_6–C_{15}, C_7–C_8, C_8–C_9, C_{10}–C_{11}, and C_{13}–C_{14}. The charge is localized (lone-pair) on C_{17}, C_{20} and on all N atoms. Similar patterns of HOMO and LUMO formation were found for compound **2** at S_0. Charge delocalization and localization behavior followed the same trend for compound **1**/**2** at S_1. It is clear from Fig. 2(a) that in the formation of HOMOs all the charge density is distributed on EDGs and the central core; for LUMOs the charge density is shifted on EWGs, revealing good intramolecular charge transfer for both the compounds.

The HOMO energies (E_{HOMO}), LUMO energies (E_{LUMO}) and HOMO–LUMO energy gaps (E_g) at S_0 and S_1 (in the brackets) states for both the compounds are tabulated in Table 1. A graphical representation of E_{HOMO} and E_{LUMO} for S_0/S_1 is shown in Fig. 3 left and right, respectively, for a more clear understanding of the E_g. E_{HOMO} of compound **1** and **2** are −5.65 eV and −5.18 eV, respectively, and are in good agreement with the experimental E_{HOMO} (−5.48 eV)[49] and the computational E_{HOMO} (−5.10 eV)[84] of the parent molecule DPNDF. The trend of E_{HOMO} and E_{LUMO}, respectively, is compound **1** (−5.65 eV, −2.93 eV) > compound **2** (−5.18 eV, −2.78 eV). A similar trend of E_{HOMO} and E_{LUMO} was found at S_1 for both the compounds.

The energy gap is theoretically expressed as the difference of the orbital energies between HOMO and LUMO whereas experimentally it is the lowest energy transition from the S_0 to the S_1 state, and termed as the band gap, which can be obtained from the absorption spectra. When electron promotion takes place from HOMO to LUMO, quantitatively E_g can be approximately the same as the optical band gap.[1,85–87] The trend in the E_g is as compound **1** (2.72 eV) > compound **2** (2.40 eV) for S_0 and for S_1 it is compound **1** (2.33 eV) > compound **2** (2.00 eV). The smaller E_g of compound **2** reveals the red shift in the absorption and emission wavelengths in comparison with compound **1**. Similarly, the lower E_g of compound **2** illuminates the high

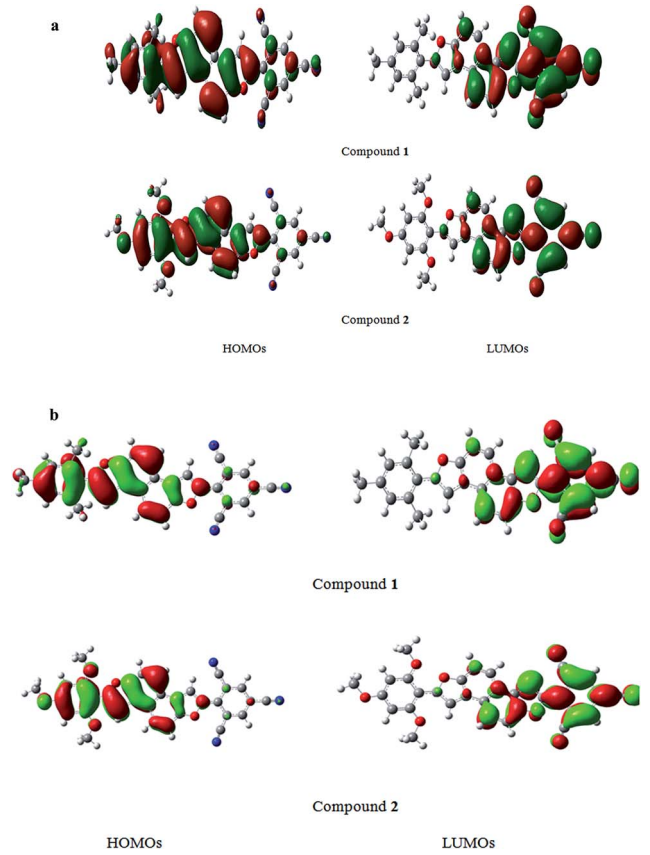

Fig. 2 (a) HOMOs and LUMOs formation patterns at ground state. (b) HOMOs and LUMOs spreading patterns at excited state.

Table 1 The E_{HOMO}[a,b], E_{LUMO} and E_g for S_0 and S_1 states (in the brackets) at the B3LYP/6-31G** and TD-B3LYP/6-31G** levels of theory

Molecule	E_{HOMO}	E_{LUMO}	E_g
Compound **1**	−5.65	−2.93	2.72
	(−5.38)	(−3.05)	(2.33)
Compound **2**	−5.18	−2.78	2.40
	(−4.86)	(−2.86)	(2.00)

[a] Experimental data (E_{HOMO} = −5.48 eV) from ref. 49. [b] Computed value (E_{HOMO} = −5.10 eV) from ref. 84.

charge transfer interaction[9,88] within the compound. A high amplitude of first hyperpolarizability (β) correlates[9,88] with a lower E_g of a compound. We anticipated that compound **2** might show larger first hyperpolarizability (β) as compared with compound **1**. It has been reported earlier that an electronic system with a smaller E_g might be more reactive[83,84] than one with a larger E_g, so compound **2** may be more reactive than compound **1**, revealing that the latter one would be more stable.

It is expected that compounds having a low-lying LUMO energy level might be thermodynamically more stable and charge transfer could not be quenched by electron loss. Moreover, according to Koopman's theorem the LUMO energy is directly proportional to the EA. The higher LUMO energy level is illuminating that the electron injection barrier would be small resulting in the improvement of charge injection ability. It can be seen from Table 1 that the value of E_{LUMO} is increased in compound **1** and **2** as compared with the computed value of E_{LUMO} (−2.17 eV)[84] for the parent molecule DPNDF, which would decrease the electron injection barrier resulting in an improvement of the electron injection. Therefore it is expected that the new compounds might be better materials as electron transporters.

3.3. Photophysical properties

The calculated absorption (λ_{abs}) and emission wavelengths (λ_{emis}), oscillator strengths (f) and HOMO–LUMO (H → L) contribution were evaluated and are tabulated in Table 2. The λ_{abs} and λ_{emis} against f are represented graphically in Fig. 4(a) and (b), respectively. Table 2 shows the maximum H → L contribution at the S_0, which is 99% from H → L for both compounds **1** and **2**. The maximum contribution of H → L for S_1 is H → L (99%) and H → L (100%) for compounds **1** and **2**, respectively. The $\lambda_{abs}/\lambda_{emis}$ have a red shift of 131/180 nm for compound **1** and 207/294 nm for compound **2**, respectively, as compared with the parent molecule of DPNDF ($\lambda_{abs}/\lambda_{emis}$ 381/427 nm) as evaluated computationally,[84] whereas compound **2** has a red shift of 76/114 nm as compared with compound **1** for $\lambda_{abs}/\lambda_{emis}$, respectively. This might be due to the strong EDGs and EWGs attached to compound **2**. The structure–property relationship revealed that by substituting the EDGs and EWGs, the λ_{abs} and the λ_{emis} have shown red shifted behavior. Compound **1** would be an orange light emitter while compound **2** would be a red light emitter.

3.4. Density of states

As remarkable electro-optical properties are attributed to a push–pull configuration in designed chemical systems, we also calculated explicit contributions for the individual parts in the form of their PDOS as shown in Fig. 5. We define three fragments for each compound: fragment one contains the phenyl ring with EWGs; fragment two is the central core (CC); and fragment three consists of the phenyl ring with EDGs. The individual fragment represents its contribution to the TDOS of the whole molecule as shown in Fig. 5 with different curves. As shown in Fig. 5, for compound **1**, the peaks from −15.0 to −8.0 eV for the valence band and from 0.0 to 7.0 eV for the conduction band are due to the similar contributions from EWGs, CC and EDGs. At the HOMO between −6.0 and −4.0 eV, the major contribution is from CC, whereas EDGs have a minor contribution. On the other hand, the EWGs take maximum part in the conduction band (−3.0 and −2.0 eV) while the CC has minimum contribution. EDGs have no contribution in the lower region of the conduction band while they have significant contribution between −1.0 to 0.0 eV and 2.0 to 7.0 eV. In TDOS the EDG contribution dominates in the lower valence bands from −13.0 to −9.0 eV and the higher conduction bands from 2.0 to 7.0 eV. The contribution of EDGs is more in the lower energy bonding molecular orbitals (−5.65 to −7.0 eV) while the

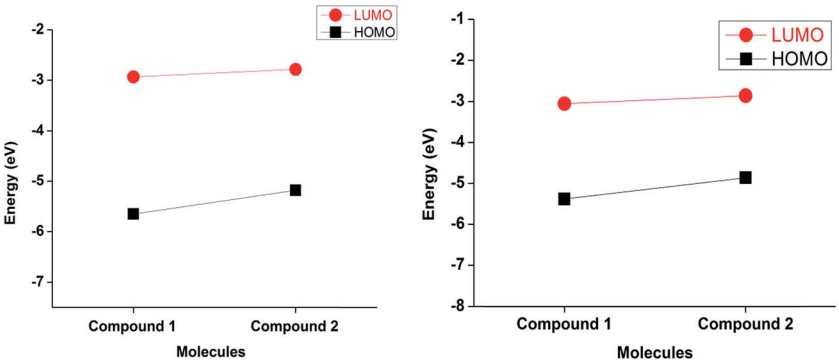

Fig. 3 Comparison of E_{HOMO} and E_{LUMO} for ground (S_0) state (left) and excited (S_1) state (right) at the B3LYP/6-31G** and TD-B3LYP/6-31G** levels of theory.

Table 2 Calculated absorption (λ_{abs}) and emission (λ_{emis}) wavelengths[a] (nm), oscillator strength (f) and HOMO–LUMO contribution for S_0 and S_1 states at the TD-DFT level of theories

Molecule	λ_{abs}	f	Contribution	λ_{emis}	f	Contribution
Compound **1**	512	0.467	H → L (99%)	607	0.373	H → L (99%)
Compound **2**	588	0.342	H → L (99%)	721	0.278	H → L (100%)

[a] Computed values (λ_{abs} = 381 nm; λ_{emis} = 427 nm) for comparison with ref. 84.

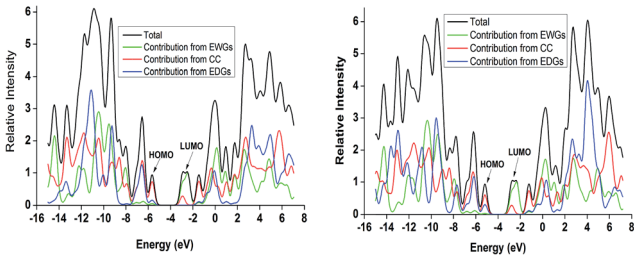

Fig. 5 Graphical representation of TDOS and PDOS for compound **1** (left) and compound **2** (right) computed at the B3LYP/6-31G** level of theory.

EWG contribution is larger in the higher energy anti-bonding molecular orbitals (−2.93 to −3.5 eV), which facilitates as easy charge transfer during the transition process of this push–pull configuration. This contribution of TDOS/PDOS from valence and conduction bands revealed good intramolecular charge transport from EDGs to EWGs. The high intramolecular charge transport from EDGs to EWGs leads to a very large value of β. A similar trend for TDOS and PDOS was found in compound **2**.

3.5. Charge transfer properties

The EA and IP are the most essential properties to calculate the charge transport barriers, and these were evaluated at the DFT/B3LYP/6-31G** level of theory. In OSMs, a lower IP and higher EA is very crucial to enhance the charge transport ability for electron and hole, respectively. The adiabatic/vertical IP (IPa/IPv) and adiabatic/vertical EA (EAa/EAv) of all derivatives were calculated and are tabulated in Table 3. A graphical comparison of the IPv, electronegativity and EAv is shown in Fig. 6 (left) to represent the results more clearly. In OFETs, the OSMs having high EAv and small IPv might be better for n-type and p-type charge injection, respectively.[89] From Table 3, it can be seen that compounds **1** and **2** have EAv of 1.63 and 1.49 eV,

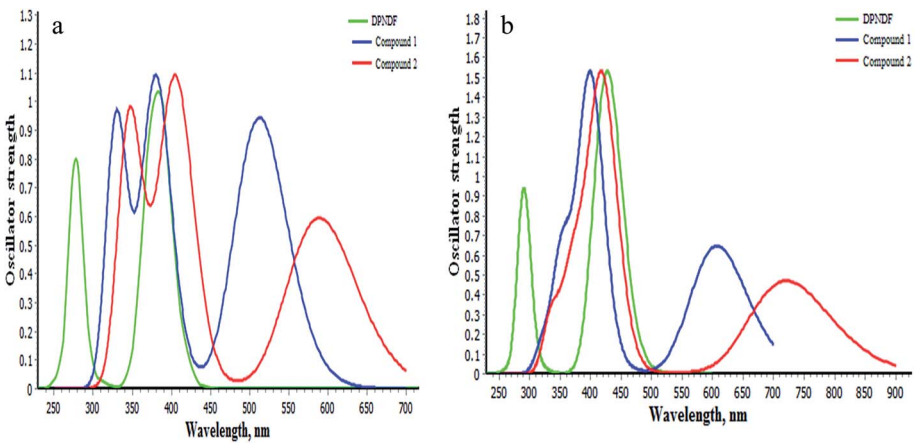

Fig. 4 (a) Computed absorption spectra and (b) computed emission spectra of compounds **1** and **2** at TD-B3LYP/6-31G** levels of theory.

Table 3 The vertical/adiabatic ionization potential and electron affinity, hole extraction potential, electron extraction potential, electronegativity and reorganization energy for hole[a] λ_h/electron λ_e at the B3LYP/6-31G** level of theory. All values are in eV

	Compound 1	Compound 2
IP (vertical)	6.85	6.37
IP (adiabatic)	6.68	6.15
HEP	6.53	5.95
EA (vertical)	1.63	1.49
EA (adiabatic)	1.76	1.61
EEP	1.87	3.36
χ	4.24	3.93
λ_h	0.32	0.42
λ_e	0.24	1.87

[a] Data for comparison (λ_h = 0.17 eV) from ref. 49.

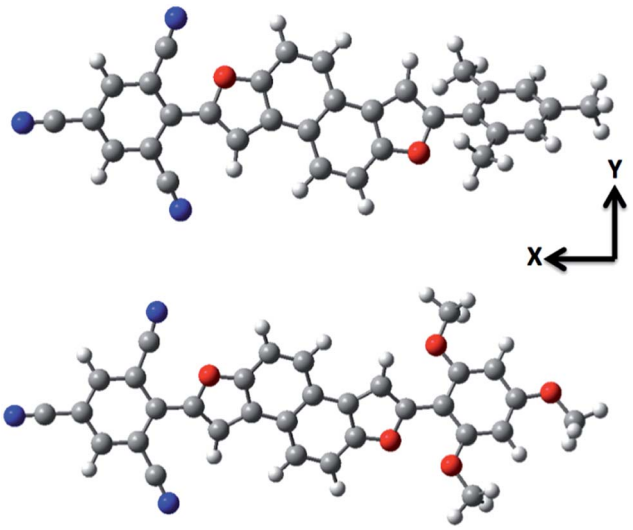

Fig. 7 The definition of the Cartesian axis for optimized structures of compounds 1 and 2.

respectively, which are higher than that of the parent molecule DPNDF (0.29 eV).[84] Thus it is expected that the new designed compounds might be much better electron transport materials as compared with DPNDF. The EAv follow the same trend as E_{LUMO} for both compounds as it has been observed that the molecule with high E_{LUMO} has the higher EAv. It can be seen from Tables 1 and 3 that compound **1** has the highest E_{LUMO} (−2.93 eV) among the two compounds and hence has the highest EAv (1.63 eV).

The reorganization energy is a quantity which is very important for estimation of the ability to carry the charge in a solid.[90,91] The reorganization energies at the B3LYP/6-31G** level of theory for electron λ_e/hole λ_h are given in Table 3. A graphical representation of hole λ_h and λ_e is shown in Fig. 6 (right) to represent the trend for further clarity. The calculated λ_h of the DPNDF is 0.17 eV (ref. 84) at the same level of theory and is in good agreement with the already computed value.[49] From Table 3, it can be seen that compounds **1** and **2** have λ_h of 0.32 and 0.42 eV, respectively, and λ_e of 0.24 and 1.87 eV, respectively. For compound **1** λ_h is higher than λ_e, whereas for compound **2** λ_h is lower than λ_e. The alteration and distortion in the bond/dihedral angles of the cation is more than that of the anion for compound **1**, resulting in more polarization[2,83] so λ_e for compound **1** is less than λ_h. On the other hand, for compound **2**, the bond/dihedral angle distortion in the anion is higher than in the cation; it might be due to this that the λ_e of compound **2** is much higher than λ_h. From this trend it is predicted that compound **1** would be good as an electron-transport material; and compound **2** might be good as a hole-transport material. The value of λ_e for compound **1** is smaller than those of diphenyl-naphtho-dithiophene (0.34 eV)[92] and oligofuran (0.40 eV),[93] which indicates that the new designed compound **1** might be more efficient as an electron transport material.

The electronegativities (χ) of the two compounds are given in Table 3. The electronegativity is the power of an atom in a molecule to attract electrons towards itself. A molecule with high electronegativity might be more efficient as an electron transport material because it can pull more electrons towards itself, resulting in high electron charge transfer.[57,71–73,94] The trend of electronegativities in compound **1** > compound **2** revealed that the former might be better as an electron transport material as compared with the latter. The reorganization

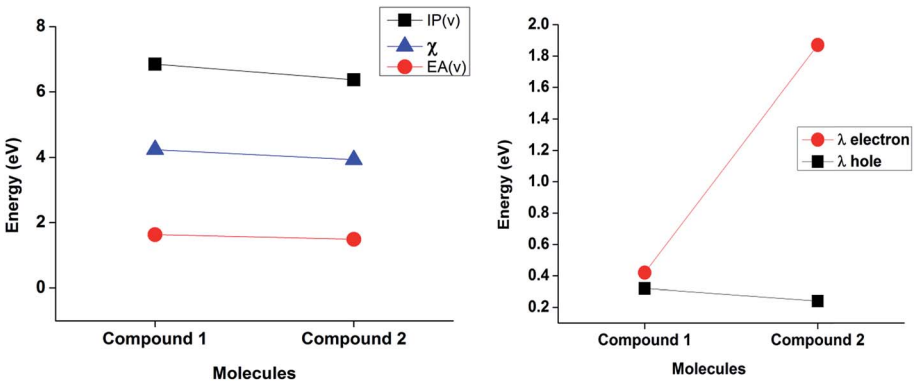

Fig. 6 Graphical representation of IPv, electronegativity and EAv (left) and of λ_h and λ_e (right) calculated at the B3LYP/6-31G** level of theory.

energies decreased with the increase in electronegativities of the compounds. It is the same trend as for E_{LUMO} and EAv of the two compounds.

3.6. First hyperpolarizability

It is well known that push–pull chemical configurations usually show remarkable NLO responses. In the present investigation taking advantage of strong push–pull configurations, we have also spotlighted the NLO responses of our designed chemical systems by calculating their static first hyperpolarizabilities. The calculated values of hyperpolarizability (β) along with their individual tensor components are shown in Table 4. A well-established electronic communication of two different parts of a push–pull molecule usually accompanies a larger amplitude of its first hyperpolarizability, which is perhaps the case in our present designed compounds **1** and **2** Fig. 7. In Table 4, it can be seen that the calculated amplitudes of first hyperpolarizability (β_{tot}) for compound **1** and **2** are significantly larger with β_{tot} values of 209.420×10^{-30} esu and 333.830×10^{-30} esu, respectively. These values of first hyperpolarizability of compound **1** and **2** are much larger than that of proto-type urea molecule [β for urea is 0.3728×10^{-30} esu]. These total hyperpolarizability values are dominated by their diagonal components (components along the dipole moment axis) of β_{xxx}. This is because there is significant charge transfer from EDGs to EWGs along the x-axis. It can be seen from Tables 1 and 4 that the first hyperpolarizability and E_g are in inverse relationship for both compounds, which supports our prediction on the basis of E_g. Thus our designed systems have significant potential for NLO applications with good stability and large first hyperpolarizability amplitudes.

3.7. Molecular simulation

In our previous study,[95] we optimized the initial geometry of the parent molecule at S_0 by a hybrid functional B3LYP along with the 6-31G** basis set using the GAUSSIAN 09 package. The crystal structure was simulated using facilities provided within the Materials Studio (MS) package using the same lattice parameters as used for the experimental crystal of DPNDF.[49] The crystal was simulated using a Molecular Mechanics (MM) simulation approach, and the energy of the crystal was minimized by the FORCITE module[96] with the $P21/c$ space group as available in the MS package, which is considered to be a good tool for this purpose. The DREIDING force field[97] was used, which is suitable for these kinds of OMs with C, H, O, and N atoms. The simulated crystal structure was found to be in good agreement with the experimentally synthesized structure (see Fig. 8). In that study we described the four pathways to compute the transfer integrals and mobility. Previously, the main computed transfer integral for the parent molecule DPNDF was 36.9 meV (ref. 95) using the GAUSSIAN package at B3LYP/6-31G** level and was closer to the available data of the same crystal 39.9 meV evaluated by the ADF program.[49] Similarly, the computed mobility was (1.1 $cm^2\ V^{-1}\ s^{-1}$), which shows good agreement with the experimentally measured value (1.30 $cm^2\ V^{-1}\ s^{-1}$). These results revealed that our adopted approach was reliable to build the crystal, and to compute the transfer integrals and mobility. In the current study, the same approach has been used to simulate the crystal structures for the new designed compounds.

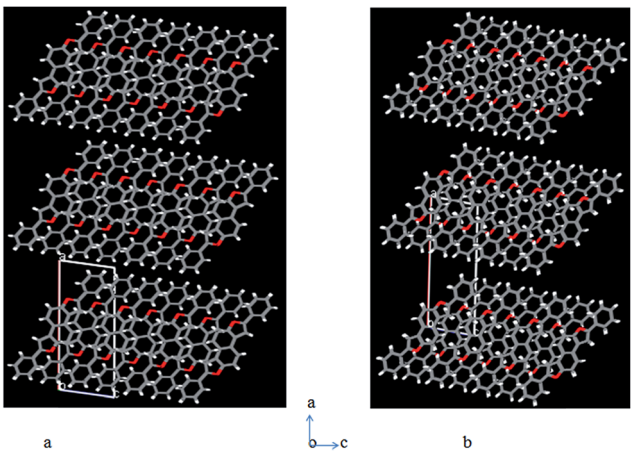

Fig. 8 Experimental (a) and simulated (b) crystal structure of DPNDF along (aoc) direction.

Table 4 The calculated values of polarizability (α) and hyperpolarizability (β) along their individual tensor components

Compound **1**			Compound **2**		
Component	a.u.	($\times 10^{-30}$) esu	Component	a.u.	($\times 10^{-30}$) esu
β_{xxx}	−24 305	200.100	β_{xxx}	−38 827	−335.500
β_{xxy}	−676	−5.841	β_{xxy}	−881	−7.613
β_{xyy}	−59	−0.509	β_{xyy}	119	1.028
β_{yyy}	7	0.0604	β_{yyy}	17	0.146
β_{xxz}	102	0.881	β_{xxz}	−362	−3.128
β_{xyz}	−90	−0.777	β_{xyz}	−103	−0.890
β_{yyz}	−30	−0.259	β_{yyz}	−8	−0.069
β_{xzz}	137	1.183	β_{xzz}	86	0.743
β_{yzz}	11	0.095	β_{yzz}	−3	−0.025
β_{zzz}	0	0.000	β_{zzz}	18	0.155
β_{tot}	24 236	209.420	β_{tot}	38 633	333.830

3.8. Transfer integrals

We have also evaluated four discrete nearest neighboring hopping pathways for the two compounds. Transfer integrals for electron and hole have been evaluated using the method expressed in eqn (2) and presented in Table 5. A graphical comparison of hole and electron transfer integrals is shown in Fig. 9(a) (left) for a more clear representation. It can be seen that some transfer integrals have negligibly small values so they are not discussed further here. The strongest hole/electron transfer integrals for compound **1** are 65.1/118.4 meV and for compound **2** are 12.9/−92 meV, respectively. Compound **1** has higher electron transfer integrals than compound **2**, revealing that compound **1** is a better electron transport material than compound **2**.

3.9. Mobility

Hole and electron mobilities of both compounds for four pathways were calculated and are tabulated in Table 5. A graphical representation of hole and electron mobilities is shown in Fig. 9(a) (right) for a more clear comparison. In our previous study[95] we computed the mobility of the parent crystal DPNDF using the direct method and found the hole mobility to be 1.1 $cm^2\ V^{-1}\ s^{-1}$, which is in good agreement with the experimentally calculated mobility of 1.30 $cm^2\ V^{-1}\ s^{-1}$ of the DPNDF.[49] We have used the same method for our current study for the four nearest neighboring molecules and found that some of the pathways have very low mobility for hole and electron; hence not discussed in the text; only the highest hole/electron mobilities for two pathways of each compound are discussed in detail here. The hole mobilities of the two pathways were found as 0.49 and 4.89×10^{-3} $cm^2\ V^{-1}\ s^{-1}$ for compound **1** and as 5.89×10^{-3} and 8.64×10^{-4} $cm^2\ V^{-1}\ s^{-1}$ for compound **2**, whereas the electron mobilities of the two pathways were found as 2.09 and 2.43 $cm^2\ V^{-1}\ s^{-1}$, for compound **1** and as 2.66×10^{-8} and 2.15×10^{-7} $cm^2\ V^{-1}\ s^{-1}$ for compound **2**. It can be seen that compound **1** exhibits the highest electron mobility of 2.43 $cm^2\ V^{-1}\ s^{-1}$ for specific 2nd pathway, which is higher than the already computed electron mobility of 1.10 $cm^2\ V^{-1}\ s^{-1}$ of the parent molecule DPNDF.

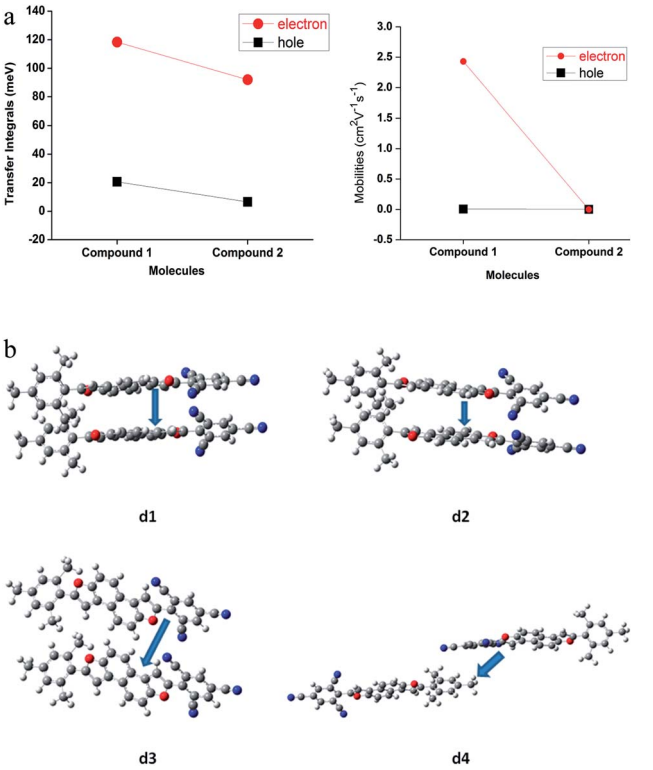

Fig. 9 (a) Graphical representation hole/electron transfer integrals (left) and mobilities (right) computed with DFT. (b) The dimers investigated in the present study to calculate the transfer integrals and mobilities.

The four pathways are shown in Fig. 9(b) for a more clear understanding of dimers packing which may affect the mobilities.[30,49] These highest electron mobility values of the 1st and 2nd pathways are in the stacking direction and might be due to the smallest distance between the two molecules of the dimers. This packing and distance allowed maximum overlapping of the orbitals ensuring enhanced mobilities, whereas the 3rd and 4th pathways have side to side packing and greater distance between two molecules, which might be the reason for the lowest mobilities.

Table 5 The transfer integrals (meV), mass centers (Å) and mobilities ($cm^2\ V^{-1}\ s^{-1}$) for hole and electron for compound **1** and **2**, computed with DFT

		Transfer integrals[c]			Mobility[c]	
Molecules	Pathways	V_h[a]	V_e	Mass centers	Hole[b]	Electron
Compound **1**	i	65.1	114.1	5.071	0.49	2.09
	ii	−20.6	118.4	5.078	4.89×10^{-3}	2.43
	iii	−2.9	6.2	7.661	4.37×10^{-6}	4.15×10^{-5}
	iv	−15.9	5.7	19.106	2.46×10^{-2}	1.85×10^{-4}
Compound **2**	i	12.9	67	5.078	5.89×10^{-3}	2.66×10^{-8}
	ii	−6.5	−92	7.661	8.64×10^{-4}	2.15×10^{-7}
	iii	2.65×10^{-3}	6.64×10^{-3}	11.969	5.84×10^{-17}	1.43×10^{-23}
	iv	−0.15738	0.21216	19.108	1.85×10^{-9}	3.79×10^{-17}

[a] V_h (39.9 meV) by other method from ref. 49. [b] Experimental hole mobility (1.30 $cm^2\ V^{-1}\ s^{-1}$) from ref. 49. [c] Computed values from ref. 95.

The highest electron mobilities for compound **1** are several times higher than DPNDF[49] and α-oligofuran[93] 0.0134 $cm^2 V^{-1} s^{-1}$, hence the former is predicted to be a good electron transport material in comparison with DPNDF and α-oligofuran. It might be due to the attached EWGs (-CN), the push–pull effect and the comprehensive intramolecular charge transfer from donor to acceptor moieties. From the highest average electron/hole intrinsic mobilities (1.13/0.13) and (6.08×10^{-8}/1.69×10^{-3}) $cm^2 V^{-1} s^{-1}$ for compound **1** and **2**, respectively, we anticipate that compound **1** is a good electron transport material; compound **2** may be a hole transport material. These results support our prediction about the same materials in terms of E_{LUMO}, IPv, EAv and reorganization energies for hole and electron.

3.10. Photostability

Molecular electrostatic surface potentials of all compounds were mapped onto a total electron density surface as shown in Fig. 10. High electron density regions and low electron density regions are shown in indigo and green, respectively. High electron density is distributed on O and N atoms in the studied systems. Previously, the photostability of organic materials has been explained on the basis of molecular electrostatic surface potentials.[56] Recently, we pointed out that more electron density distributed on the system would favor enhanced photostability.[98] In our last study we observed that in the parent molecule DPNDF the high electron density is distributed on oxygen atoms[95] (see Fig. S2 of the ESI†). By substituting the EDGs and EWGs, the photostability was augmented in our designed molecules. The substitution of $-CH_3$ and –CN at the outer phenyl rings in compound **1** improved the photostability compared with the parent DPNDF molecule. High electron density distribution in compound **2** covered more area due to the $-OCH_3$ and –CN than in compound **1**, revealing that the former would be more photostable than the latter, that is due to strong EDGs ($-OCH_3$) attached with compound **2**. We noticed that by increasing the size and strength of EDGs, the photostability might be enhanced. Higher electron density in compound **2** would decrease the oxidation resulting in improved photostability, which is in good agreement with our previous study.[99]

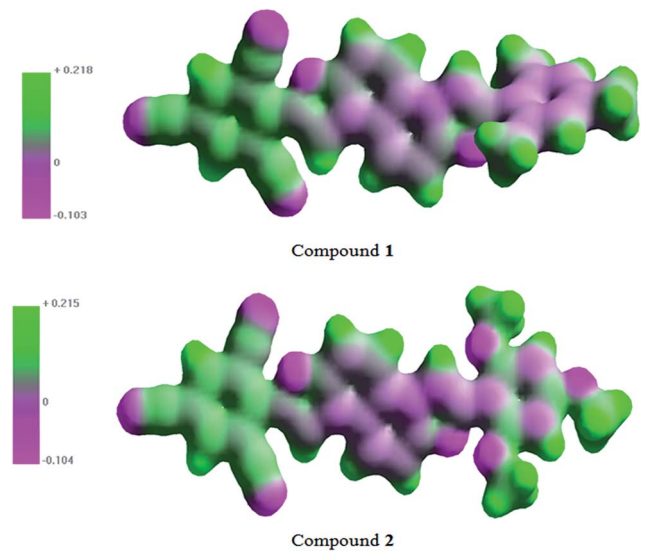

Fig. 10 Molecular electrostatic potential surfaces of the two compounds.

4. Conclusions

Push–pull configurations have shown interesting effects for tuning the electro-optical properties of compounds **1** and **2**. In the light of our present DFT investigation, we can draw the following interesting conclusions:

1. The two designed novel compounds have higher EAv values as compared with their parent molecule DPNDF.

2. The absorption and emission spectra of designed compounds **1** and **2** have a red shift as compared with their parent molecule. This is because of well-established communication between donor and acceptor parts. The HOMOs and LUMOs in both the studied compounds are delocalized as well as localized on the central core and EWGs, respectively. The EWGs take part in the establishment of LUMOs only. The HOMO energies are in good agreement with the experimentally estimated HOMO of the parent molecule DPNDF.

3. The influence of the push–pull parts has been investigated by calculating their total and partial density of states (DOS).

4. Taking advantage of strong push–pull configurations, our designed chemical systems have also been rationalized as efficient NLO materials with significantly larger amplitudes of first hyperpolarizability for compounds **1** and **2**.

5. The first hyperpolarizability and HOMO–LUMO energy gap are in inverse relationship for compounds **1** and **2**.

6. The electron transfer integrals and electron mobility have been enhanced significantly in compound **1** by introducing the $-CH_3$ and –CN groups, respectively. So it is predicted that compound **1** would be a good electron transport material as compared to compound **2** and the parent molecule DPNDF.

7. The photostability has been enhanced significantly in compound **2** by introducing the $-OCH_3$ and –CN groups, because of enriched electron density distributed on these groups. As a result it is predicted that compound **2** would be more stable than compound **1**.

Hence, we expect that these compounds would serve as excellent candidates for OFET, OLET and OLED applications with enhanced photostability.

Acknowledgements

The authors are grateful to the Ministry of Education/Universiti Teknologi Malaysia (UTM) for providing funding *via* project Q.J130000.2526.06H15 for the successful execution of this project and to King Khalid University (KKU) for providing the support and facilities to complete the research study.

References

1 Y. Li, L.-Y. Zou, A.-M. Ren and J.-K. Feng, *Comput. Theor. Chem.*, 2012, **981**, 14.
2 A. Irfan, R. Cui, J. Zhang and L. Hao, *Chem. Phys.*, 2009, **364**, 39.
3 A. É. Masunov and P. M. Zorkii, *J. Struct. Chem.*, 1992, **33**, 423.
4 S. Ananthavel and M. Manoharan, *Chem. Phys.*, 2001, **269**, 49.
5 A. Irfan, A. G. Al-Sehemi and S. Muhammad, *Synth. Met.*, 2014, **190**, 27.
6 A. Irfan, A. G. Al-Sehemi and M. S. Al-Assiri, *Comput. Theor. Chem.*, 2014, **1031**, 76.
7 A. Irfan, A. G. Al-Sehemi and M. S. Al-Assiri, *J. Fluorine Chem.*, 2014, **157**, 52.
8 A. Irfan, A. G. Al-Sehemi and M. S. Al-Assiri, *J. Mol. Graphics Modell.*, 2013, **44**, 168.
9 H. Alyar, *Rev. Adv. Mater. Sci.*, 2013, **34**, 79.
10 P. Srinivasan, T. Kanagasekaran and R. Gopalakrishnan, *Cryst. Growth Des.*, 2008, **8**, 2340.
11 M. Rao, R. Ponce Ortiz, A. Facchetti, T. J. Marks and K. S. Narayan, *J. Phys. Chem. C*, 2010, **114**, 20609.
12 I. Osaka, T. Abe, M. Shimawaki, T. Koganezawa and K. Takimiya, *ACS Macro Lett.*, 2012, **1**, 437.
13 H. E. Katz, *J. Mater. Chem.*, 1997, **7**, 369.
14 G. Horowitz and M. E. Hajlaoui, *Adv. Mater.*, 2000, **12**, 1046.
15 C. R. Newman, C. D. Frisbie, D. A. da Silva Filho, J.-L. Brédas, P. C. Ewbank and K. R. Mann, *Chem. Mater.*, 2004, **16**, 4436.
16 C. W. Tang and S. A. VanSlyke, *Appl. Phys. Lett.*, 1987, **51**, 913.
17 P. K. H. Ho, J.-S. Kim, J. H. Burroughes, H. Becker, S. F. Y. Li, T. M. Brown, F. Cacialli and R. H. Friend, *Nature*, 2000, **404**, 481.
18 F. Padinger, R. S. Rittberger and N. S. Sariciftci, *Adv. Funct. Mater.*, 2003, **13**, 85.
19 K. Niimi, H. Mori, E. Miyazaki, I. Osaka, H. Kakizoe, K. Takimiya and C. Adachi, *Chem. Commun.*, 2012, **48**, 5892.
20 A. W. Hofmann, *Proc. R. Soc. London*, 1856, **8**, 1.
21 IUPAC, *Compendium of Chemical Terminology (the Gold Book)*, ed. A. D. McNaught and A. Wilkinson, 2nd edn, 1997.
22 P. v. R. Schleyer, *Chem. Rev.*, 2005, **105**, 3433.
23 J.-L. Brédas, D. Beljonne, V. Coropceanu and J. Cornil, *Chem. Rev.*, 2004, **104**, 4971.
24 J.-L. Brédas, J. Cornil, D. Beljonne, D. A. dos Santos and Z. Shuai, *Acc. Chem. Res.*, 1999, **32**, 267.
25 J. Cornil, D. A. dos Santos, X. Crispin, R. Silbey and J. L. Brédas, *J. Am. Chem. Soc.*, 1998, **120**, 1289.
26 J. L. Bredas and G. B. Street, *Acc. Chem. Res.*, 1985, **18**, 309.
27 A. Warshel and M. Karplus, *J. Am. Chem. Soc.*, 1974, **96**, 5677.
28 S.-C. Yang, W. Graupner, S. Guha, P. Puschnig, C. Martin, H. R. Chandrasekhar, M. Chandrasekhar, G. Leising, C. Ambrosch-Draxl and U. Scherf, *Phys. Rev. Lett.*, 2000, **85**, 2388.
29 A. Irfan, M. Nadeem, M. Athar, F. Kanwal and J. Zhang, *Comput. Theor. Chem.*, 2011, **968**, 8.
30 A. Irfan, A. G. Al-Sehemi, S. Muhammad and J. Zhang, *Aust. J. Chem.*, 2011, **64**, 1587.
31 M. S. Wrackmeyer, M. Hein, A. Petrich, J. Meiss, M. Hummert, M. K. Riede and K. Leo, *Sol. Energy Mater. Sol. Cells*, 2011, **95**, 3171.
32 S. Das, S. P. Senanayak, A. Bedi, K. S. Narayan and S. S. Zade, *Polymer*, 2011, **52**, 5780.
33 J. A. Letizia, S. Cronin, R. P. Ortiz, A. Facchetti, M. A. Ratner and T. J. Marks, *Chem.–Eur. J.*, 2010, **16**, 1911.
34 F. Buonocore and A. Matteo, *Theor. Chem. Acc.*, 2009, **124**, 217.
35 Q.-X. Wu, Y. Geng, Y. Liao, X.-D. Tang, G.-C. Yang and Z.-M. Su, *Theor. Chem. Acc.*, 2012, **131**, 1.
36 K. N. N. Unni, S. Dabos-Seignon and J.-M. Nunzi, *J. Mater. Sci.*, 2006, **41**, 317.
37 P. Pingel, A. Zen, D. Neher, I. Lieberwirth, G. Wegner, S. Allard and U. Scherf, *Appl. Phys. A*, 2009, **95**, 67.
38 H. Koezuka, A. Tsumura and T. Ando, *Synth. Met.*, 1987, **18**, 699.
39 Y. Miyata, T. Nishinaga and K. Komatsu, *J. Org. Chem.*, 2005, **70**, 1147.
40 Y. Miyata, M. Terayama, T. Minari, T. Nishinaga, T. Nemoto, S. Isoda and K. Komatsu, *Chem.–Asian J.*, 2007, **2**, 1492.
41 O. Gidron, A. Dadvand, Y. Sheynin, M. Bendikov and D. F. Perepichka, *Chem. Commun.*, 2011, **47**, 1976.
42 C.-C. Wu, W.-Y. Hung, T.-L. Liu, L.-Z. Zhang and T.-Y. Luh, *J. Appl. Phys.*, 2003, **93**, 5465.
43 K. Kadac, M. J. Bosiak and J. Nowaczyk, *Synth. Met.*, 2012, **162**, 1981.
44 M. Watanabe, W.-T. Su, Y. J. Chang, T.-H. Chao, Y.-S. Wen and T. J. Chow, *Chem.–Asian J.*, 2013, **8**, 60.
45 M. Nakano, S. Shinamura, Y. Houchin, I. Osaka, E. Miyazaki and K. Takimiya, *Chem. Commun.*, 2012, **48**, 5671.
46 M. Nakano, K. Niimi, E. Miyazaki, I. Osaka and K. Takimiya, *J. Org. Chem.*, 2012, **77**, 8099.
47 K. Mitsudo, J. Harada, Y. Tanaka, H. Mandai, C. Nishioka, H. Tanaka, A. Wakamiya, Y. Murata and S. Suga, *J. Org. Chem.*, 2013, **78**, 2763.
48 H. Chen, W. Delaunay, J. Li, Z. Wang, P.-A. Bouit, D. Tondelier, B. Geffroy, F. Mathey, Z. Duan, R. Réau and M. Hissler, *Org. Lett.*, 2013, **15**, 330.
49 C. Mitsui, J. Soeda, K. Miwa, H. Tsuji, J. Takeya and E. Nakamura, *J. Am. Chem. Soc.*, 2012, **134**, 5448.
50 A. R. Chaudhry, R. Ahmed, A. Irfan, A. Shaari and A. G. Al-Sehemi, *Mater. Chem. Phys.*, 2013, **138**, 468.
51 P. J. Stephens, F. J. Devlin, C. F. Chabalowski and M. J. Frisch, *J. Phys. Chem.*, 1994, **98**, 11623.
52 A. D. Becke, *J. Chem. Phys.*, 1993, **98**, 5648.
53 C. Lee, W. Yang and R. G. Parr, *Phys. Rev. B: Condens. Matter Mater. Phys.*, 1988, **37**, 785.
54 E. Cho, C. Risko, D. Kim, R. Gysel, N. Cates Miller, D. W. Breiby, M. D. McGehee, M. F. Toney, R. J. Kline and J.-L. Bredas, *J. Am. Chem. Soc.*, 2012, **134**, 6177.
55 T. Sajoto, S. P. Tiwari, H. Li, C. Risko, S. Barlow, Q. Zhang, J.-Y. Cho, J.-L. Brédas, B. Kippelen and S. R. Marder, *Polymer*, 2012, **53**, 1072.
56 A. Irfan, J. Zhang and Y. Chang, *Theor. Chem. Acc.*, 2010, **127**, 587.

57 R. Bauernschmitt and R. Ahlrichs, *Chem. Phys. Lett.*, 1996, **256**, 454.
58 C. Van Caillie and R. D. Amos, *Chem. Phys. Lett.*, 2000, **317**, 159.
59 F. Furche and R. Ahlrichs, *J. Chem. Phys.*, 2002, **117**, 7433.
60 G. Scalmani, M. J. Frisch, B. Mennucci, J. Tomasi, R. Cammi and V. Barone, *J. Chem. Phys.*, 2006, **124**, 094107.
61 J. E. Lee, G. C. Choi, N. G. Park, Y. K. Ha and Y. S. Kim, *Curr. Appl. Phys.*, 2004, **4**, 675.
62 M. C. Zwier, J. M. Shorb and B. P. Krueger, *J. Comput. Chem.*, 2007, **28**, 1572.
63 E. Li, A. Kim, L. Zhang, *Journal of Student Computational Chemistry*, Spring, 2007, vol. 1, North Carolina School of Science and Mathematics.
64 N. E. Gruhn, D. A. da Silva Filho, T. G. Bill, M. Malagoli, V. Coropceanu, A. Kahn and J.-L. Brédas, *J. Am. Chem. Soc.*, 2002, **124**, 7918.
65 J. R. Reimers, *J. Chem. Phys.*, 2001, **115**, 9103.
66 A. Irfan, R. Cui and J. Zhang, *Theor. Chem. Acc.*, 2009, **122**, 275.
67 V. Coropceanu, T. Nakano, N. E. Gruhn, O. Kwon, T. Yade, K.-i. Katsukawa and J.-L. Brédas, *J. Phys. Chem. B*, 2006, **110**, 9482.
68 B. C. Lin, C. P. Cheng, Z.-Q. You and C.-P. Hsu, *J. Am. Chem. Soc.*, 2004, **127**, 66.
69 A. Troisi and G. Orlandi, *Chem. Phys. Lett.*, 2001, **344**, 509.
70 S. Yin, Y. Yi, Q. Li, G. Yu, Y. Liu and Z. Shuai, *J. Phys. Chem. A*, 2006, **110**, 7138.
71 M. J. Frisch, G. W. Trucks, H. B. Schlegel, G. E. Scuseria, M. A. Robb, J. R. Cheeseman, G. Scalmani, V. Barone, B. Mennucci, G. A. Petersson, H. Nakatsuji, M. Caricato, X. Li, H. P. Hratchian, A. F. Izmaylov, J. Bloino, G. Zheng, J. L. Sonnenberg, M. Hada, M. Ehara, K. Toyota, R. Fukuda, J. Hasegawa, M. Ishida, T. Nakajima, Y. Honda, O. Kitao, H. Nakai, T. Vreven Jr, J. E. Peralta, F. Ogliaro, M. Bearpark, J. J. Heyd, E. Brothers, K. N. Kudin, V. N. Staroverov, R. Kobayashi, J. Normand, K. Raghavachari, A. Rendell, J. C. Burant, S. S. Iyengar, J. Tomasi, M. Cossi, N. Rega, J. M. Millam, M. Klene, J. E. Knox, J. B. Cross, V. Bakken, C. Adamo, J. Jaramillo, R. Gomperts, R. E. Stratmann, O. Yazyev, A. J. Austin, R. Cammi, C. Pomelli, J. W. Ochterski, R. L. Martin, K. Morokuma, V. G. Zakrzewski, G. A. Voth, P. Salvador, J. J. Dannenberg, S. Dapprich, A. D. Daniels, Farkas, J. B. Foresman, J. V. Ortiz, J. Cioslowski and D. J. Fox, *Gaussian 09 Revision A.02*, Gaussian Inc., Wallingford, CT, 2009.
72 C. Dehu, F. Meyers and J. L. Bredas, *J. Am. Chem. Soc.*, 1993, **115**, 6198.
73 S. Muhammad, M. R. S. A. Janjua and Z. Su, *J. Phys. Chem. C*, 2009, **113**, 12551.
74 S. Muhammad, C. Liu, L. Zhao, S. Wu and Z. Su, *Theor. Chem. Acc.*, 2009, **122**, 77.
75 S. Muhammad, H. Xu, Y. Liao, Y. Kan and Z. Su, *J. Am. Chem. Soc.*, 2009, **131**, 11833.
76 H.-L. Xu, Z.-R. Li, Z.-M. Su, S. Muhammad, F. L. Gu and K. Harigaya, *J. Phys. Chem. C*, 2009, **113**, 15380.
77 S. Muhammad, H. Xu, M. R. S. A. Janjua, Z. Su and M. Nadeem, *Phys. Chem. Chem. Phys.*, 2010, **12**, 4791.
78 S. Muhammad, T. Minami, H. Fukui, K. Yoneda, R. Kishi, Y. Shigeta and M. Nakano, *J. Phys. Chem. A*, 2012, **116**, 1417.
79 D. L. Wang, H. L. Xu, Z. M. Su, S. Muhammad and D. Y. Hou, *ChemPhysChem*, 2012, **13**, 1232.
80 R.-L. Zhong, H.-L. Xu, S. Muhammad, J. Zhang and Z.-M. Su, *J. Mater. Chem.*, 2012, **22**, 2196.
81 S. Muhammad, H. Xu, Z. Su, K. Fukuda, R. Kishi, Y. Shigeta and M. Nakano, *Dalton Trans.*, 2013, 15053.
82 A. B. Ahmed, H. Feki, Y. Abid, H. Boughzala and A. Mlayah, *J. Mol. Struct.*, 2008, **888**, 180.
83 Y. Xiaodi, L. Qikai and S. Zhigang, *Nanotechnology*, 2007, **18**, 424029.
84 A. R. Chaudhry, R. Ahmed, A. Irfan, A. Shaari, H. Maarof and A. G. Al-Sehemi, *Sains Malays.*, 2014, **43**, 867.
85 P. J. Hay, *J. Phys. Chem. A*, 2002, **106**, 1634.
86 A. Curioni, W. Andreoni, R. Treusch, F. J. Himpsel, E. Haskal, P. Seidler, C. Heske, S. Kakar, T. Van Buuren and L. J. Terminello, *Appl. Phys. Lett.*, 1998, **72**, 1575.
87 S. Y. Hong, D. Y. Kim, C. Y. Kim and R. Hoffmann, *Macromolecules*, 2001, **34**, 6474.
88 V. Arjunan, P. S. Balamourougane, C. V. Mythili and S. Mohan, *J. Mol. Struct.*, 2011, **1003**, 92.
89 Y. Zhang, X. Cai, Y. Bian, X. Li and J. Jiang, *J. Phys. Chem. C*, 2008, **112**, 5148.
90 R. A. Marcus, *Rev. Mod. Phys.*, 1993, **65**, 599.
91 J. L. Brédas, J. P. Calbert, D. A. da Silva Filho and J. Cornil, *Proc. Natl. Acad. Sci. U. S. A.*, 2002, **99**, 5804.
92 Y. Yi, L. Zhu and J.-L. Brédas, *J. Phys. Chem. C*, 2012, **116**, 5215.
93 S. Mohakud, A. P. Alex and S. K. Pati, *J. Phys. Chem. C*, 2010, **114**, 20436.
94 Y. Ie, Y. Umemoto, M. Okabe, T. Kusunoki, K.-i. Nakayama, Y.-J. Pu, J. Kido, H. Tada and Y. Aso, *Org. Lett.*, 2008, **10**, 833.
95 A. R. Chaudhry, R. Ahmed, A. Irfan, A. Shaari and A. G. Al-Sehemi, *Sci. Adv. Mater.*, 2014, **6**, 1727.
96 W. H. Baur and D. Kassner, *Acta Crystallogr., Sect. B: Struct. Sci.*, 1992, **48**, 356.
97 S. L. Mayo, B. D. Olafson and W. A. Goddard, *J. Phys. Chem.*, 1990, **94**, 8897.
98 A. Irfan and J. Zhang, *Theor. Chem. Acc.*, 2009, **124**, 339.
99 A. Irfan, R. Cui, J. Zhang and M. Nadeem, *Aust. J. Chem.*, 2010, **63**, 1283.